Making Heterometallic Metal-Metal Bonds in Keggin-Type Polyoxometalates by a Six-Electron Reduction Process

Clément Falaise, Gabrielle Mpacko Priso, Nathalie Leclerc, Mohamed Haouas, Emmanuel Cadot

Clustering Molybdenum Substituted Keggin-type Silicotungstate by Six-Electron Reduction Process

Clément Falaise,*[a] Gabrielle Mpacko Priso,[a] Nathalie Leclerc, [a] Mohamed Haouas,[a] and Emmanuel Cadot [a]

[a] *Institut Lavoisier de Versailles, CNRS, UVSQ, Université Paris-Saclay, 45 avenue des Etats-Unis, 78035, Versailles, France.*

† Electronic Supplementary Information (ESI) available: materials and methods, additional figures and tables, CCDC 2121920. See DOI: 10.1039/x0xx00000x

Polyoxometalates (POMs) represent a promising class of molecular electron reservoirs, however their multi-electron reduction gives rise to intricate physical-chemical phenomena that must be fully understood for their future use in energy-storage devices. Herein, we show that bulk electrolysis of the archetypal Keggin-type POM $[Si(W^{VI}_2Mo^{VI}O_{10})(W^{VI}_3O_{10})_3]^{4-}$ in aqueous solution leads to the six-electron reduced derivative $[Si(W^{IV}_2Mo^{IV}O_7(H_2O)_3)(W^{VI}_3O_{10})_3]^{4-}$ in which the mixed-metal triad acts as a storage unit for six electrons and six protons. X-ray diffraction analysis and multinuclear NMR (^{183}W and ^{95}Mo) of solution are consistent with the presence of three metal-metal bonds which make this highly reduced species the first example of mixed-metal "heteropoly brown" polyanion. Remarkably, this entity results from a fast clustering process compared to that observed for the entirely W-based analogue. Besides, $[Si(W^{IV}_2Mo^{IV}O_7(H_2O)_3)(W^{VI}_3O_{10})_3]^{4-}$ can be further reduced through multi-electronic events, while its full oxidation through irreversible redox process restores the initial structure of the oxidized parent ion. Based on cloud point measurements of a non-ionic surfactant, we evidence that the clustering process has dramatic consequences on the solution behaviour of the POM, cancelling its super-chaotropic character. These fundamental results pave the way for applications using the massive electron-storage properties of mixed-metal POMs.

Introduction

General understanding of electron transfer chemistry coupled to molecular transformation represents an intense field of research leading to breakthroughs in molecular engineering, catalysis or energy storage.[1–4] Among the redox-active molecules, polyoxometalates (POMs) behave strikingly as electron reservoir. They represent an unique class of compounds, that are built from group VI transition-metal centres (Mo^{VI} or W^{VI}) assembled by oxygen atoms within a large variety of compositions and structures.[5,6] The relationships between their molecular structure and their redox properties are quite well described for their first reduced states.[7,8] These weakly reduced POMs obtained by successive quasi-reversible reduction steps, are known as the so-called "heteropoly blues" due to their deep-blue colour in solution that is a direct consequence of the optically-activated electron hopping over the metal centres.[9–13] When POMs are reduced by a larger number of electrons (four or more), intricate phenomena including isomerization, protonation, disproportionation or aggregation could take place, that can be either a benefit or a drawback for their use in energy-related applications.[3,14,15] In context, comprehensive study of the physical-chemical events occurring along their electrochemical reduction appears as crucial from a fundamental aspect but also for *i*) their rational integration as active components in batteries (Li-ion, Na-ion, or redox flow), and for *ii*) their use as redox mediators in electro(photo)catalytic processes.[3,14]

The Keggin-type silicotungstate α-$[Si(W^{VI}_3O_{10})_4]^{4-}$ (abbreviated SiW_{12}-0), containing a central SiO_4 tetrahedron surrounded by four triads $\{M_3O_{13}\}$ mutually connected through corner-shared junctions, represents a popular charge carrier used in ground-breaking electrochemical devices.[15–18] Nevertheless, pioneered works have revealed that its electrolysis at controlled potential in acidic solution can lead to well-defined six-electron reduced POMs $[Si(W^{IV}_3O_7(H_2O)_3)(W^{VI}_3O_{10})_3]^{4-}$ (notated SiW_{12}-VI') in which 5*d*-electrons are localized in three metal-metal bonds forming a W^{IV} based trinuclear cluster.[19–21] Formation of such Janus-like POMs, named "heteropoly browns" arises from disproportionation processes of "heteropoly blues" which lead to an electron-rich clustered triad coexisting in the POM framework with three other electron-poor triads.[20,22] Interestingly, additional tungstate ions can be condensed onto the electron-rich triad, leading to 20-tungstate polyanions.[23] So far, no mixed-metal based Keggin anions have been identified to form "heteropoly browns" by electrochemical reduction in solution, while few is known on the solution properties of these "heteropolybrown" derivatives.[19,24–29]

Herein, we report the electrochemical preparation of the first mixed-metal Mo/W "heteropoly brown" (Fig. 1) and its structural characterization using single-crystal X-ray diffraction and ^{95}Mo, ^{183}W and ^{29}Si NMR in solution, evidencing unambiguously the mixed-metal Mo/W triad clustered as storage unit for containing six electrons and six protons as three meta-metal bonds and three aqua ligands, respectively. The formation of this brown derivative $[Si(W^{IV}_2Mo^{IV}O_7(H_2O)_3)(W^{VI}_3O_{10})_3]^{4-}$ (notated **SiW_{11}Mo-VI'**) has been monitored using electrochemical methods and UV-vis spectroscopy, highlighting the importance of Mo addenda on the clustering process that leads to the localization of the charges within the metal-oxo framework. Besides, the redox behaviour of this "heteropoly brown"

species has been investigated in aqueous solution, revealing rich redox behaviour which involves both the electron-poor {SiW^{VI}_9} subunit and the electron-rich {$W^{IV}_2Mo^{IV}$} core. At last, we evaluate the solvation properties of **SiW_{11}Mo-VI'** using a method based on the cloud point measurement of a non-ionic surfactant. This experiment reveals that the clustering process induces the lost of super-chaotropic character of the Keggin anion.

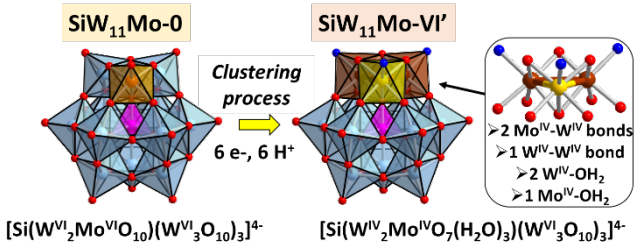

Fig. 1. Schematic representation showing the formation of "heteropoly brown" SiW_{11}Mo-VI' induced by the six-electron reduction of molybdenum mono-substituted α-Keggin type silicotungstate SiW_{11}Mo-0 in acidic solution. The molybdenum doping strategy facilitates the "heteropoly brown" formation with the selective reduction of mixed metal triad. Light blue polyhedral: W^{VI}; brown polyhedra: W^{IV}; orange polyhedra: Mo^{VI}; yellow polyhedral: Mo^{IV}; red spheres: oxygen; blue spheres: terminal water molecule; pink polyhedral: Si.

Results and discussion

Cyclic and steady-state voltammetric analysis

The presence of Mo addenda within the silicotungstate is known to favour the electrochemical reduction by increasing the redox potential of the first electron transfers.[7,30] This behaviour led us to hypothesize that such conditions could make easier deep electrochemical reduction by favouring the formation of the "heteropoly brown" derivatives. Then, we investigated the electrochemical behaviour of the molybdenum mono-substituted Keggin anion $[Si(W^{VI}_2Mo^{VI}O_{10})(W^{VI}_3O_{10})_3]^{4-}$ (SiW_{11}Mo-0) in 0.5 M HCl. The use of acidic condition is known to facilitate the POM reduction thanks to proton-coupled electron transfers,[7] occurring in the formation of "heteropoly browns".
So far, all the reported electrochemical studies on this polyanion only described the two first reversible mono-electronic events, labelled A and B (see Fig. 2A *black curve* and Fig. S2†), observed at +385 and -335 mV *vs* Ag/AgCl, respectively.[31] The first electron transfer (A event), involves the reduction of the single Mo centre while the second electrochemical B event leads to the formation of the SiW_{11}Mo-II species containing formally one W^V and one Mo^V reduced centres. Interestingly, the cyclic voltammogram extended between -900 and 1000 mV *vs* Ag/AgCl potential range (Fig. 2A *red curve*) reveals one irreversible multi-electronic reduction wave (labelled C) located at -540 mV *vs* Ag/AgCl. Steady-state voltammogram obtained using rotating working glassy carbon electrode shows this reduction wave involves about 4-5 electrons (Fig. 2B *red curve*), however accurate determination of the number of electrons involved in this C event remains difficult due to the existence of an additional close multi-electronic cathodic event (D) observed at -700 mV *vs* Ag/AgCl. Interestingly the anodic back-potential sweep reveals an irreversible and intense oxidation peak at positive potentials above +400 mV *vs* Ag/AgCl (Fig. 2A *red curve* and Fig. S2), notated Ox which only occurs if the C event has taken place. Such an irreversible electrochemical behaviour is characteristic of a chemical transformation driven by electrons transfer process and could be the signature of the "heteropoly browns" formation.[32] Consistency, cycling experiments between -650 and 0 mV *vs* Ag/AgCl (Fig. S3) indicate unambiguously that the C event involves the chemical conversion from "heteropoly blue" to "heteropoly brown" species. Indeed, cycling provokes important modifications of the CV such as i) the progressive disappearance of the B event, ii) the decrease of the cathodic peak C and concomitantly iii) the increase of its anodic peak. This suggests the existence of an electrochemical coupled chemical reaction mechanism, involving the chemical transformation of the *"*heteropoly blue*"* species into the "heteropoly brown" **SiW_{11}Mo-VI'**. This overall clustering process starting from the reduction of the *"*heteropoly blue*"* SiW_{11}Mo-II can be expressed by a first quasi-reversible proton-coupled redox reaction involving six protons and four electrons according to the Equation 1, followed by a second step which corresponds to the irreversible chemical transformation from VI to VI' (Equation 2). Then, according to the Nernst equation, the apparent redox potential of the C event should vary of -88.5 mV per *p*H unit (Equations 3 and 4). Experimentally, the potential of the redox event C varies from about -94 mV per *p*H unit in the 0.3-4.8 *p*H range (Fig. 2B) giving fairly good agreement with the expected value.

$$\mathrm{II} + 4\,\mathrm{e}^- + 6\,\mathrm{H}^+ \rightleftarrows \mathrm{VI} \quad (\mathbf{1}) \qquad\qquad \mathrm{VI} \rightarrow \mathrm{VI}' \quad (\mathbf{2})$$

$$E_{II/VI} = E^0_{II/VI} + \frac{RT}{4F}\ln\frac{[II][H^+]^6}{[VI]} \quad (\mathbf{3})$$

$$E_{1/2_{II/VI}} = E^0_{II/VI} - 0.0885\,pH \quad (\mathbf{4})$$

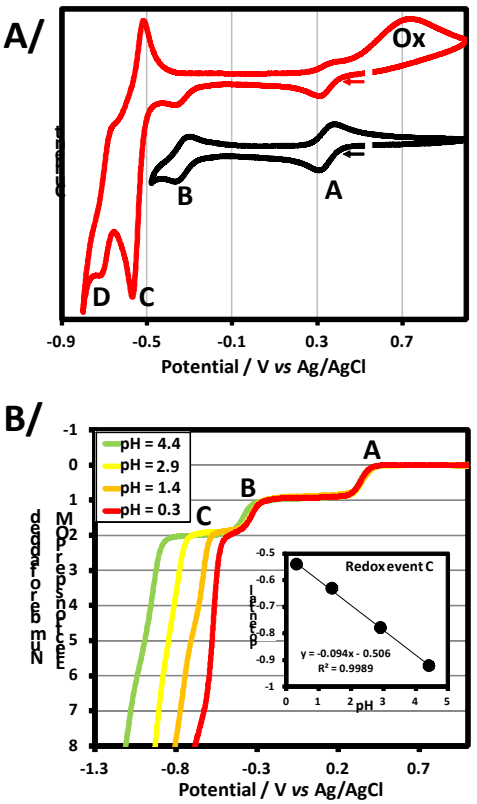

Fig. 2. A/ Cyclic voltammograms of $[Si(W^{VI}_2Mo^{VI}O_{10})(W^{VI}_3O_{10})_3]^{4-}$ in 0.5 M aqueous HCl solution recorded in the potential range -480 to 1000 mV *vs* Ag/AgCl (black curve) and the potential range -800 to 1000 mV *vs* Ag/AgCl (red curve). [POM] = 2 mM; WE: glassy carbon; REF: Ag/AgCl; CE: Pt; scan rate: 100 mV/s. B/ Comparison of the steady-state voltammograms obtained at different pH, illustrating the C event varies to about -94 mV per *p*H unit as shown in the insert. The current has been normalized to the number of electrons involved per POM unit in the different reduction processes. [POM] = 2 mM; WE: rotating carbon glassy electrode (2000 rpm); REF: Ag/AgCl; CE: Pt; scan rate: 100 mV/s.

Electro-synthesis and structural analysis of {SiW$_{11}$Mo}-VI'

Preliminary voltammetric studies revealed that the reduction of the two-electron reduced led to the formation of "heteropoly brown" at moderate low potential (about -540 mV at *p*H 0.3). Then, questions arise about the localization of the six electrons within POM framework. To elucidate this, preparative bulk electrolysis has been performed and the resulting compound has been fully characterized by NMR and single-crystal X-ray diffraction.
Controlled potential electrolysis of the oxidized parent polyanion $K_4[Si(W^{VI}_2Mo^{VI}O_{10})(W^{VI}_3O_{10})_3].16H_2O$ (7.5 g; 2.3 mmol) in HCl (0.5 M) was carried out under argon flow, using Toray carbon fiber paper as working electrode (applied potential: -570 mV *vs* Ag/AgCl) and a graphite counter electrode separated from working-electrode compartment by a sintered-glass disk. In such conditions, the bulk electrolysis allowed to consume charges, corresponding to the expected six electrons per polyanion. Crystalline dark solid $Rb_4[Si(W^{IV}_2Mo^{IV}O_7(H_2O)_3)(W^{VI}_3O_{10})_3].10H_2O$, notated Rb_4.**SiW$_{11}$Mo-VI'**.$10H_2O$, was isolated in good yield (~80 %) by addition of RbCl. The use of KCl or CsCl instead of RbCl, gives poor-quality crystals. Single-crystal X-ray diffraction analysis of Rb_4.**SiW$_{11}$Mo-VI'**.$10H_2O$ is consistent with a non-centrosymmetric $P2_1$ space group (Table S1 for further details) allowing the localization of the Keggin-type polyanion **SiW$_{11}$Mo-VI'**, rubidium cations and water molecules. The "heteropoly brown" structure retains the main characteristic expected for the α-Keggin type arrangement (Fig. 1B). However, one of the four triads $\{M_3O_{13}\}$ is drastically modified (Fig. 3A), and exhibits three metal centres bounded together by short metal-metal bonds ($d_{M\text{-}M}$ = 2.5601(6)-2.5674(6) Å). Importantly, the structural refinement indicates these three M^{IV} sites (see BVS calculation, Fig. S1) are occupied by 2/3 of W and 1/3 of Mo, consistent with a triangular $\{W^{IV}_2Mo^{IV}O_{13}\}$ cluster in which the Mo atom is statistically disordered with the W atoms over the three positions of the metal centres. The W···W distances in the other triads fall in the 3.35-3.42 Å range as usually observed for non-bonding contacts in oxidized silicotungstates.[33,34] The shrinking of the metal-metal distances within the electron-rich triad induces also important modifications of the M-O bond distances and M-O-M angle values compared with those generally observed for the oxidized analogue (Fig. 3 and Table S2). This intramolecular reorganization can be described as the displacement of the three metal atoms within a rigid oxygen close-packing, retaining an almost perfect octahedral site within the reduced triad $\{W^{IV}_2Mo^{IV}O_{13}\}$.

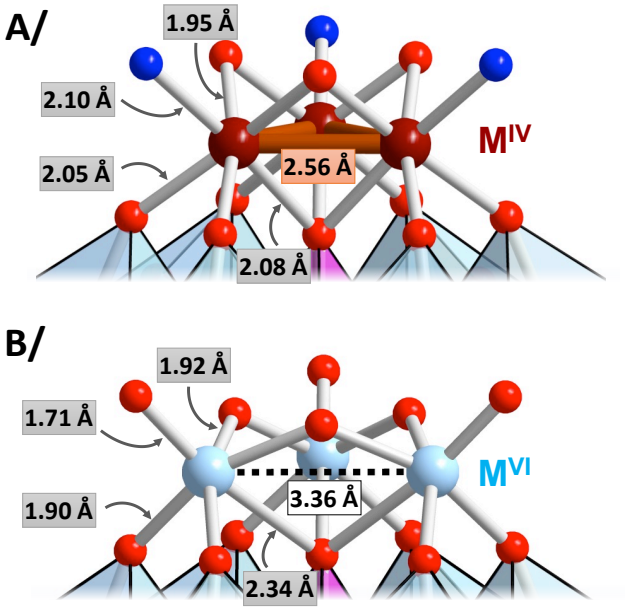

Fig. 3. A/ Illustration of the electron-rich triad $\{W^{IV}_2Mo^{IV}O_{13}\}$ observed in the X-ray crystal structure of the compound Rb_4.**SiW_{11}Mo-VI'**.10H_2O, highlighting the presence of the metal-metal bonds between the tetravalent metal centres and the M^{IV}-O distances. B/ Illustration of the oxidized triad $\{W^{VI}_3O_{13}\}$ observed in the silicotungstate $[SiW_{12}O_{40}]^{4-}$[31,32]. Red spheres: oxygen; blue spheres: terminal water molecules; brown spheres: M^{IV} with M = 1/3 Mo and 2/3 W; Light blue spheres: W^{VI}.

Nonetheless, another important alteration lies in the M-O distances involving terminal oxygen atoms (Fig. 3). These distances fall in the 2.074(8)-2.132(8) Å range, and appears rather consistent with terminal oxygen atoms belonging to water molecules, as confirmed by bond valence sum calculations (Fig. S1). In the three remaining oxidized triads, the terminal oxo groups are doubly bound to the W^{VI} ($d_{W\text{-}O}$ = 1.709(8)-1.727(7) Å). Actually, the inner displacement of three M^{IV} due to the formation of the metal-metal bonds induces a shortening of about 0.26 Å of the M-O bond distances involving the μ_4-oxo group belonging to the SiO_4 tetrahedra. We also observed some significant changes in the M-O-M angles, especially those involving the μ_2-oxo groups in the triads, which are closed to about 82° in Rb_4.**SiW_{11}Mo-VI'**.10H_2O while they exhibit larger values of around 122° for the oxidized POM. All these structural modifications induced by the six-electron reduction have important consequences on the M-O vibrations as evidenced by the comparison of the IR spectra of the compound Rb_4.**SiW_{11}Mo-VI'**.10H_2O with that of the oxidized parent ion (Fig. S11).

To provide further support of the X-ray diffraction structural interpretation, we performed multinuclear ^{29}Si, ^{95}Mo and ^{183}W NMR in acidic aqueous solution (0.1 M DCl/D_2O; [**SiW_{11}Mo-VI'**] = 100 mM). The ^{95}Mo NMR spectrum exhibits a single signal featuring a highly deshielded Mo nucleus by approximately 1650 ppm compared to the signal observed for the oxidized POM SiW_{11}Mo-0 (Fig. 4B and S9). This ^{95}Mo resonance observed at 1660 ppm falls in the typical chemical shift range expected for Mo^{IV} but appears at higher chemical shift than those observed in the incomplete-cubane $\{Mo_3O_4\}$ clusters.[35,36] This result confirms entirely the presence of the Mo centre belonging to the triangular six electron-reduced $\{M^{IV}_3O_{13}\}$ based cluster as proposed above by analysis of the crystallographic data. The ^{95}Mo quadripolar nucleus is highly sensitive to the anisotropy of the local electric field gradient and consequently the magnitude of the ^{95}Mo NMR linewidth gives information about the degree of symmetry of the Mo coordination sphere.[35] The ^{95}Mo NMR linewidth decreases from 1100 Hz to approximately 300 Hz by the reduction of the Mo^{VI} into Mo^{IV} resulting of the formation of the "heteropoly brown" derivative. Such a result highlights nicely the increasing of the symmetry of the octahedral site containing the Mo^{IV} ion (pseudo O_h) with respect to that in the oxidized POM (C_{4v} symmetry). In addition, the ^{183}W NMR spectrum exhibits in the typical region of the W^{VI} five resonances of relative intensities 2:2:1:2:2 (Fig. 4C) which is consistent with a $\{SiW_9\}$ subunit in the C_s symmetry. Furthermore, 2D-INADEQUATE NMR experiment was performed to assign these ^{183}W NMR signals by establishing their connectivities through $^2J_{W\text{–}O\text{–}W}$ coupling constants (Fig. S8). Then, ^{183}W NMR resonances of the three pairs of equivalent W^{VI} adjacent to the M^{IV}-based triad (notated W3, W4, W5; Fig. 4) are observed in the range -100 and -110 ppm, while the three remaining W^{VI} centres corresponding to the W2 pair and to the W1 single atom, located on the opposite site of the electron-rich triad are slightly deshielded at -88 and -98 ppm, respectively. All these resonances are observed within the usual chemical shift range for oxidized W^{VI} centres, as already found in other "heteropoly browns" $[Si(W^{IV}_3O_7(H_2O)_3)(W^{VI}_3O_{10})_3]^{n-}$ with X = Si, B or H_2. [19,28] Besides, the spin-spin couplings $^2J_{W\text{–}O\text{–}W}$ have been determined for almost the tungsten-tungsten connections and fall in the 6-7 Hz range for the edge-shared W-O-W junctions and in the 20-22 Hz for the corner-shared junctions. Importantly, the ^{183}W NMR spectrum contains

an additional strongly deshielded ^{183}W signal at +1375 ppm with a relative intensity of 2, which is assigned to the two equivalent W^{IV} centres (Fig. 4C). Furthermore, this signal contains a W-W coupling ($^{2}J_{W-O-W}$ = 15.3 Hz) corresponding to the corner-shared junctions with the W5 pair. It must be noted the nuclei of the W^{IV} centres in $SiW_{11}Mo$-VI' are less deshielded than those observed by Pope and co-worker for W^{IV} in SiW_{12}-VI' (+1544.6 ppm, $^{2}J_{W-O-W}$ = 15.2 Hz).[19] This observation follows the trend previously reported on a series of trinuclear mixed clusters $[W_{3-x}Mo_xO_2(CH_3COO)_6]^{2+}$ (with x = 0-3) in which the ^{183}W chemical shift decreases when the Mo^{IV} content increases, while conversely the ^{95}Mo signals downfield shift when W^{IV} content increases in the triad.[37] The magnitude of the paramagnetic contribution to the nuclear screening could be tentatively explained by the electronic distribution of the *d* electrons within the bonding metal-metal orbitals which should be denser at the Mo atoms than near W atoms. This generates a slightly lower formal oxidation state for the single Mo centre and a slightly higher oxidation state for both adjacent W centres in the mixed reduced triad. At last, the single ^{29}Si NMR signal in $[Si(W^{IV}_2Mo^{IV}O_7(H_2O)_3)(W^{VI}_3O_{10})_3]^{4-}$ is only slightly shifted (-2 ppm), due to the weak distortion of the SiO_4 tetrahedron in the "heteropoly brown" (Fig. S10 and Table S2).

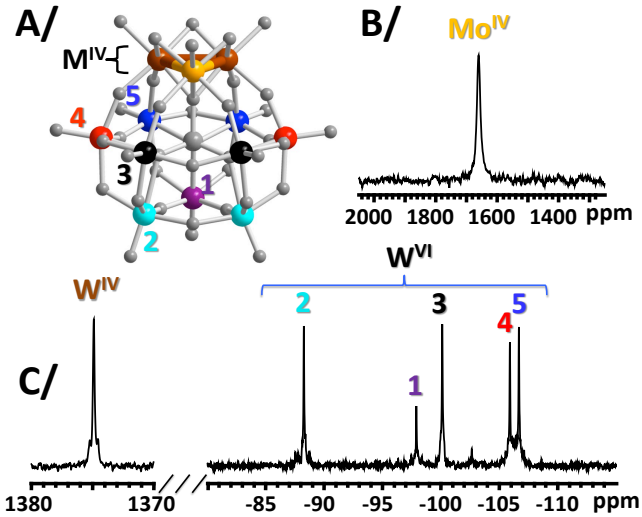

Figure 4. ^{95}Mo and ^{183}W NMR characterizations of the "heteropoly brown" **$SiW_{11}Mo$-VI'**. A) Illustration of the structure highlighting the equivalent metal centers. B) NMR signal of the reduced Mo^{IV}. C) NMR signals of the W centers and their attribution.

Progress of the electrolysis by UV-Vis and voltammetry

Comparison of the steady-state voltammograms of SiW_{12}-0 and $SiW_{11}Mo$-0 highlights the presence of single Mo centre into the Keggin-type POM favours the "heteropoly brown" formation (Fig. 5). From a thermodynamic point of view, **$SiW_{11}Mo$-VI'** is easier to prepare because its formation occurring at the redox event C is observed at potential higher than the redox couple IV/II of the silicotungstate Keggin-type anion. However, the main difference concerns the mechanism and kinetics of the clustering process.

In the case of the Keggin-type silicotungstate SiW_{12}-0, it was reported that the four-electron reduced species SiW_{12}-IV is thermodynamically unstable in acidic conditions and consequently undergoes disproportionation process (2 IV → II + VI') to lead to the mixture of SiW_{12}-VI' and SiW_{12}-II.[20,22] This clustering process appears very slow with respect to electrochemical time window, because this is not observed on

low scan rates voltammograms, or on repeated cycling experiments (Fig. S4). In contrast, the cyclic and steady-state voltammetry investigations (Fig. 1 and Fig. S3) reveal that the formation of the mixed metal "heteropoly brown" **$SiW_{11}Mo$-VI'** proceeds through remarkably fast process. The rate constant of the overall clustering process cannot be simply determined due to multiple reasons including overlapping with redox events of the reaction product. However, the formation of brown derivative **$SiW_{11}Mo$-VI'** clearly take place in time window shorter than those of the rotating disk electrode voltammetry because the anodic current of the event C vary linearly with $\sqrt{\omega}$ where ω is rotation rate (Fig. S5), meaning the electron-transfer is only limited by the mass transport at the electrode. Therefore, it can be concluded that the overall reduction-driven chemical transformation from $SiW_{11}Mo$-0 to **$SiW_{11}Mo$-VI'** occurs within few *ms* in 0.5 M HCl.

The chemical transformation from "heteropoly blue" to "heteropoly brown" depend also upon proton concentration (*p*H) and the global charge density of the POM, however we demonstrate herein that the metalate composition of the Keggin anion have much more dramatic consequences on the clustering process. Actually, the clustering pathway of the Mo mono-substituted Keggin anion-type POM $SiW_{11}Mo$-0 (Equation 1 and 2) does not

involved a disproportionation process as for the fully W-based Keggin $[Si(W^{VI}_3O_{10})_4]^{4-}$ or the metatungstate polyanion $[H_2(W^{VI}_3O_{10})_4]^{6-}$.[20,22,32] For the later, simulating cyclic voltammetric data showed that formation of the corresponding "heteropoly brown" derivative $[H_2(W^{IV}_3O_7(H_2O)_3)(W^{VI}_3O_{10})_3]^{6-}$ occurs through a slow disproportionation rate (k = 0.008 s^{-1}).[32]

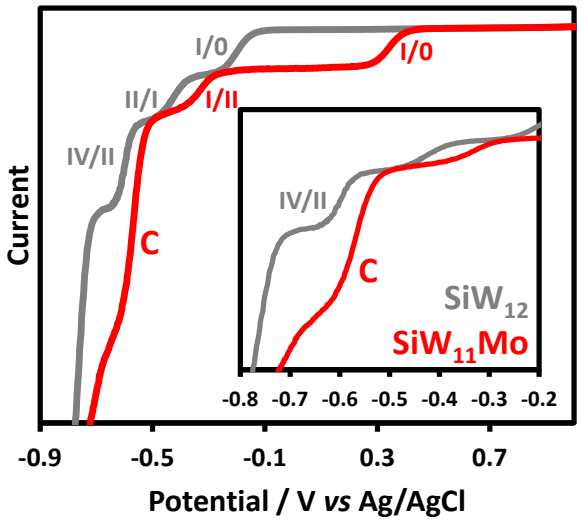

Fig. 5. Comparison of the steady-state voltammograms of $[Si(W^{VI}_2Mo^{VI}O_{10})(W^{VI}_3O_{10})_3]^{4-}$ (red curve) and $[Si(W^{VI}_3O_{10})_4]^{4-}$ (grey curve) in 0.5 M aqueous HCl solution. [POM] = 2 mM; WE: rotating carbon glassy electrode (2000 rpm); REF: Ag/AgCl; CE: Pt; scan rate: 100 mV/s.

To give further insights about the formation process of the **SiW_{11}Mo-VI'**, we engaged *in-situ* study to characterize the bulk solution over the electrochemical reduction process through UV-vis spectroscopy and steady-state voltammetric analysis. Controlled potential electrolysis of the 2 mM oxidized parent polyanion $[Si(W^{VI}_2Mo^{VI}O_{10})(W^{VI}_3O_{10})_3]^{4-}$ in 0.5 M HCl, was performed applying a potential of -0.57 V *vs* Ag/AgCl.

Before the reduction, the pale-yellow solution of oxidized polyanion exhibits only significant absorption below 400 nm corresponding to ligand-to-metal charge transfer (Fig. 6A). Upon electrochemical reduction process, drastic colour changes are observed, as evidenced by the evolution of the UV-vis spectra (Fig. 6A).

After the reduction by 1 *F* (adding of 1e- per POM), the dark purple solution contains exclusively one electron reduced $[Si(W^{VI}_2Mo^{V}O_{10})(W^{VI}_3O_{10})_3]^{5-}$ as confirmed by steady-state voltammogram that exhibits similar profile to the oxidized form, except a positive offset of the current (Fig. 6B). Because Mo^{6+} is more reducible than W^{6+}, the first electron fills the Mo d_{xy}-type non-bonding orbital. The electronic signature of SiW_{11}Mo-I is featured by an absorption band located at 500 nm (ε = 1000 $M.cm^{-1}$) and a shoulder at 750 nm, as previously observed by Sanchez,[38] and is mostly attributed to *d-d* transitions with some contributions arising from $Mo^{V}\rightarrow W^{VI}$ intervalence charge transfer (IVCT). Reduction by 2 *F* induces a deep blue coloration of the solution, and the UV-vis signature is featured by three wide absorption bands located at 470, 620 and 1100 cm^{-1} (Fig. 6A). Undoubtedly, the band at 1100 cm^{-1} corresponds to $W^{V}\rightarrow W^{VI}$ IVCT and the electronic nature of these absorptions is similar to that depicted for the one- or two-electron reduced Keggin polyoxotungstates.[13] Further reduction produces absorbance decreasing, giving a clear brown solution after reduction by 6 *F*. Such a spectrum is characterized by a weak and broad absorption band observed between 500 to 750 nm (Figure 6A), corresponding probably to *d-d* transitions of the Mo^{IV} and W^{IV} of the electron-rich triad (ε = 220 $M.cm^{-1}$ at 700 cm^{-1}; ε = 290 $M.cm^{-1}$ at 550 cm^{-1}). The evolution of the steady-state voltammogram of the solutions (Figure 6B) indicates the POM undergoes a molecular rearrangement for reduction superior to 2 *F*, because a novel redox event appears (Ox event) while both A and B redox events disappear. All these observations indicate that the formation of the "heteropoly brown" **SiW_{11}Mo-VI'** during the bulk electrolysis proceeds directly from the six-electron "heteropoly blue" intermediate SiW_{11}Mo-VI which converts through a fast electronic and structural rearrangement into the "heteropoly brown" derivative.

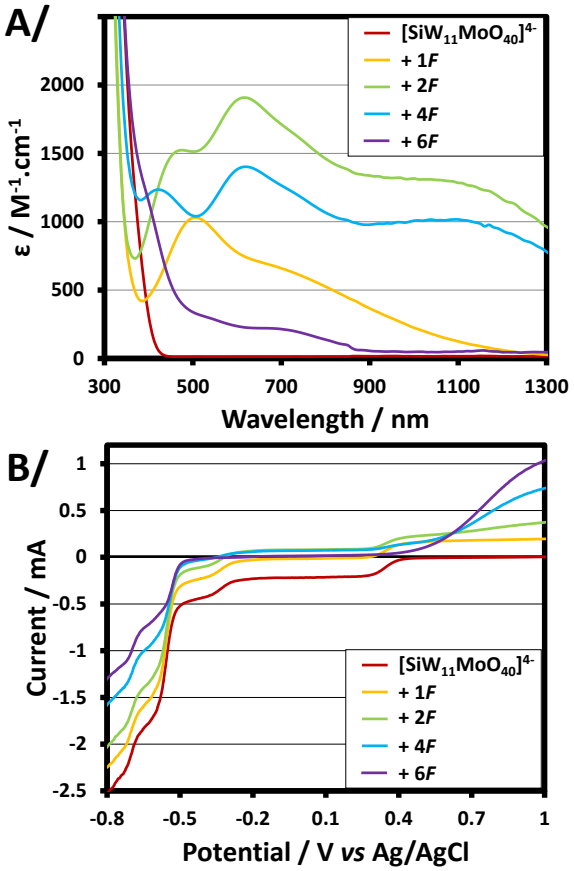

Fig. 6. Evolution of the UV-vis spectrum (A) and the steady-state voltammogram (B) during the bulk electrolysis of acidic aqueous solution containing molybdenum mono-substituted Keggin anion with various reduction levels. [POM] = 2 mM; WE: rotating carbon glassy electrode (2000 rpm); REF: Ag/AgCl; CE: Pt; scan rate: 100 mV/s; *p*H = 0.3.

Redox behavior of SiW_{11}Mo-VI'

The redox properties of preformed **SiW_{11}Mo-VI'** brown derivative have been studied in 0.5 M aqueous HCl solution and the corresponding cyclic voltammograms are reported in Fig. 7 and Fig. S7.

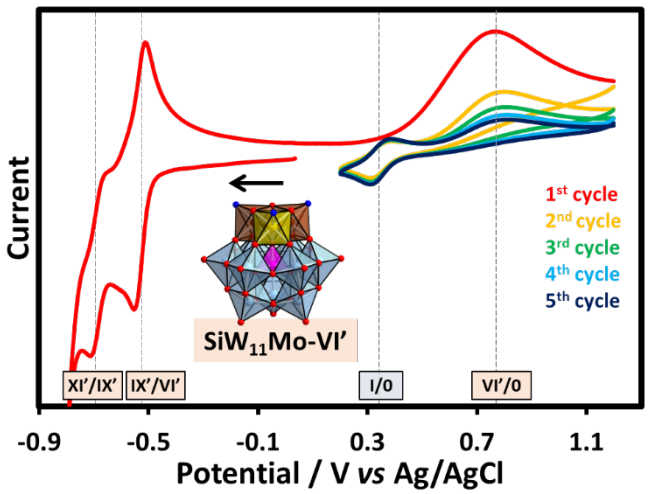

Fig. 7. Cyclic voltammograms of the $[SiW_{11}MoO_{37}(H_2O)_3]^{4-}$ in 0.5 M HCl recorded in the potential range -800 to 1200 mV *vs* Ag/AgCl. [POM] = 2 mM; WE: glassy carbon; REF: Ag/AgCl; CE: Pt; scan rate: 100 mV/s.

Scanning from 0 to –800 mV *vs* Ag/AgCl revealed the presence of two nearly reversible multi-electronic redox waves. The variation of the peak currents of the first multi-electronic event exhibits a fair linear dependence upon square

root of the potential scan rate, consistent with a diffusion-controlled electron-transfer kinetic (Fig. S6). The number of electrons involved in each redox event has been determined using rotating disk electrode. The first wave, observed at -540 mV, corresponds to the transfer of three electrons to the **$SiW_{11}Mo$-VI''** leading to the IX' reduced species, resulting of three delocalized "blue" electrons and six electrons firmly trapped within metal-metal bonds of the $\{W^{IV}_2Mo^{IV}\}$ triad. Then, a second quasi-reversible wave observed at -700 mV *vs* Ag/AgCl involves two electrons for giving a 11 electron-containing Keggin anions, distributed as six "brown" electrons and five "blue" electrons. Then, oxidation of the brown derivative $[Si(W^{IV}_2Mo^{IV}O_7(H_2O)_3)(W^{VI}_3O_{10})_3]^{4-}$ into $[Si(W^{VI}_2Mo^{VI}O_{10})(W^{VI}_3O_{10})_3]^{4-}$ through a six-electron transfer is characterized by a non-reversible anodic large peak (VI'/0) which spread from 0.5 to 1.2 V *vs* Ag/AgCl. The swiping back cycling between +1.1 and +0.2 V *vs* Ag/AgCl revealed $SiW_{11}Mo$-0 is fully restored as evidenced by the reappearance of the redox wave I/0. This demonstrates that the integrity of the POM is maintained during the massive electron transfers.

Solvation properties of $SiW_{11}Mo$-VI'

One of the most striking supramolecular properties of POMs arises from their ability to form highly stable systems with neutral organic moieties including cyclodextrins, micelles or large biomolecules.[39–43] The strength of such hybrid associations is related to the chaotropic (water-structure breaking) character of the POM.[44] The chaotropicity of **$SiW_{11}Mo$-VI'** and its oxidized parent $SiW_{11}Mo$-0 has been evaluated by investigating the evolution of the cloud point temperature (CPT) of non-ionic surfactants C8E4 (tetraethylene glycol monooctyl ether; 60 mM) upon addition of POMs (from 0 to 20 mM). This method was previously used to classify POMs in Hofmeister series.[43] When the concentration of oxidized form $SiW_{11}Mo$-0 increases, a significant increase of the CPT is observed indicating strong interactions between C8E4 surfactant-based micelles and POMs (see Figure 8). For instance, the CPT of C8E4 increases of about 60 °C as the concentration of $SiW_{11}Mo$-0 is varied in the 0-20 mM range. Actually, The CPT curve of $SiW_{11}Mo$-0 is similar to that reported with SiW_{12}-0, ranging therefore $SiW_{11}Mo$-0 as a super-chaotrope entities in the extended Hofmeister series (Fig. S12).[45,46] In contrast, CPT curve varies only very weakly in presence of **$SiW_{11}Mo$-VI'** (Fig. 8). For a solution containing 20 mM of **$SiW_{11}Mo$-VI'**, the CP rises only by 2 °C. This order of magnitude is typically those observed for small chaotrope ions (e.g. SCN^-; Fig. S12). All these observations show that the heteropoly brown **$SiW_{11}Mo$-VI'** exhibits a very weak ability to interact with non-ionic organic matters.

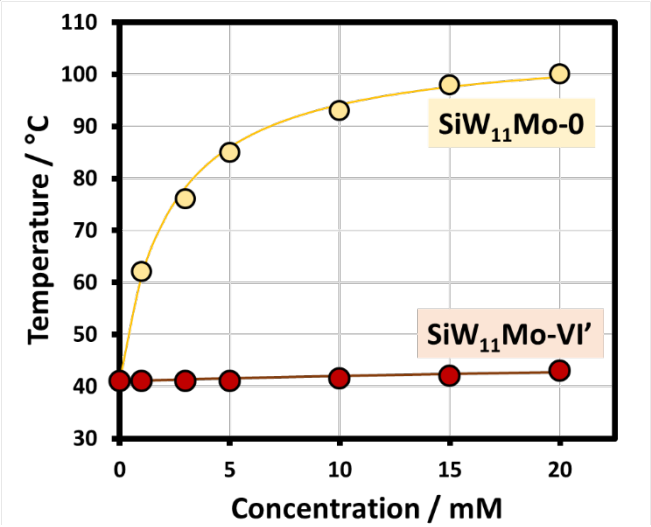

Fig. 8. Cloud point evolution of 60 mM tetraethylene glycol monooctyl ether as a function of salt concentration for the molybdenum substituted Keggin-type silicotungstates exhibiting a global charge of 4- : $[Si(W^{VI}_2Mo^{VI}O_{10})(W^{VI}_3O_{10})_3]^{4-}$ (clear yellow dots) and $[Si(W^{IV}_2Mo^{IV}O_7(H_2O)_3)(W^{VI}_3O_{10})_3]^{4-}$ (brown dots). The solid lines represent the Langmuir isotherm fits, allowing comparison with Keggin-type polyoxotungstates and classical chaotropic ions (see Fig. S12 for more details).

Several reports highlight that the global charge-density of POMs represents the main contributor of their chaotropic character.[40,43,45] Although they have the same charge-density, the "heteropoly brown" $[Si(W^{IV}_2Mo^{IV}O_7(H_2O)_3)(W^{VI}_3O_{10})_3]^{4-}$ and its oxidized parent $[Si(W^{VI}_2Mo^{VI}O_{10})(W^{VI}_3O_{10})_3]^{4-}$ exhibit very contrasted solution behaviours. This can be understood by considering the nature of the POM/solution interface. In the $SiW_{11}Mo$-0 anion, a loosely bound and disordered water molecules of the hydration shell at the origin of the super-chaotropic effect arises from the exclusive presence of the low charge density outer metal-oxo groups. For the **$SiW_{11}Mo$-VI'** derivative, the situation differs significantly because of the three exposed terminal water molecules linked to the mixed-metal electron-rich triad. Therefore, these coordinated water molecules strengthen and order

the interactions with water molecules of the hydration shell through the formation of hydrogen bonds. As a consequence of this local structuring effect of the hydration shell, the chaotropicity of the **$SiW_{11}Mo$-VI'** decrease dramatically. This result demonstrates for the first time that the reduction-induced aquation of the POMs surface modified in a large extend their hydration properties.

Conclusion

The reduction process of the molybdenum mono-substituted Keggin anion $[Si(W^{VI}_2Mo^{VI}O_{10})(W^{VI}_3O_{10})_3]^{4-}$ has been investigated in acidic solution. The massive electron transfer on this POM provokes its molecular transformation through a fast clustering process, leading to six-electron reduced POM formulated as $[Si(W^{IV}_2Mo^{IV}O_7(H_2O)_3)(W^{VI}_3O_{10})_3]^{4-}$. Structural characterizations have revealed the charges (six electrons and six protons) are stored in the mixed metal Mo/W triad exhibiting three metal-metal bonds, while the other W-based triads remain almost unchanged. This "heteropoly brown" can be oxidized directly to regenerate the $[Si(W^{VI}_2Mo^{VI}O_{10})(W^{VI}_3O_{10})_3]^{4-}$. In addition, study on the hydration properties of the "heteropoly brown" evidences the key role of the protonation upon chaotropic character of POMs.
Besides, the facile preparation of this electro-active $[Si(W^{IV}_2Mo^{IV}O_7(H_2O)_3)(W^{VI}_3O_{10})_3]^{4-}$ "heteropoly brown" in which three water molecules are expected labile enough to create coordinatively unsaturated sites for potential applications in the field of the activation and electrocatalytic conversion of small molecules or organic substrates.[47–49]

Data availability

All experimental and characterisation data in this article are available in the ESI.

Author Contributions

C. Falaise – conceptualization, investigation (synthesis, electrochemistry, X-ray diffraction, cloud point), writing (original draft), and funding acquisition. G. Mpacko Priso – investigation (electrochemistry). N. Leclerc – investigation (synthesis, elemental analysis). M. Haouas – investigation (NMR) and writing (review & editing). E. Cadot – conceptualization and writing (review & editing).

Conflicts of interest

There are no conflicts to declare.

Acknowledgements

Authors gratefully acknowledge financial supports from LabEx CHARMMMAT (grant number ANR-11-LBX-0039), University of Versailles Saint-Quentin, and the CNRS (MOMENTUM-grant).

Notes and references

1 M. J. Chalkley, P. Garrido-Barros and J. C. Peters, *Science*, 2020, **369**, 850–854.
2 B. E. Petel, W. W. Brennessel and E. M. Matson, *J. Am. Chem. Soc.*, 2018, **140**, 8424–8428.
3 J.-J. Chen, M. D. Symes and L. Cronin, *Nat. Chem.*, 2018, **10**, 1042–1047.
4 N. von Wolff and M. Robert, *Chem. Rec.*, 2021, **21**, 2095–2106.
5 M. Pope, *Heteropoly and Isopoly Oxometalates*, Springer-Verlag, Berlin Heidelberg, 1983.
6 D.-L. Long, R. Tsunashima and L. Cronin, *Angew. Chem. Int. Ed.*, 2010, **49**, 1736–1758.
7 M. Sadakane and E. Steckhan, *Chem. Rev.*, 1998, **98**, 219–238.
8 T. Ueda, *ChemElectroChem*, 2018, **5**, 823–838.
9 M. T. Pope and G. M. Varga, *Inorg. Chem.*, 1966, **5**, 1249–1254.
10 M. Kozik and L. C. W. Baker, in *Polyoxometalates: From Platonic Solids to Anti-Retroviral Activity*, eds. M. T. Pope and A. Müller, Springer Netherlands, Dordrecht, 1994, pp. 191–202.
11 N. Suaud, A. Gaita-Ariño, J. M. Clemente-Juan, J. Sánchez-Marín and E. Coronado, *J. Am. Chem. Soc.*, 2002, **124**, 15134–15140.
12 D. C. Duncan and C. L. Hill, *Inorg. Chem.*, 1996, **35**, 5828–5835.
13 C. Sanchez, J. Livage, J. P. Launay and M. Fournier, *J. Am. Chem. Soc.*, 1983, **105**, 6817–6823.

14 H. Wang, S. Hamanaka, Y. Nishimoto, S. Irle, T. Yokoyama, H. Yoshikawa and K. Awaga, *J. Am. Chem. Soc.*, 2012, **134**, 4918–4924.
15 L. MacDonald, B. Rausch, M. D. Symes and L. Cronin, *Chem. Commun.*, 2018, **54**, 1093–1096.
16 B. Rausch, M. D. Symes, G. Chisholm and L. Cronin, *Science*, 2014, **345**, 1326–1330.
17 J. Friedl, M. V. Holland-Cunz, F. Cording, F. L. Pfanschilling, C. Wills, W. McFarlane, B. Schricker, R. Fleck, H. Wolfschmidt and U. Stimming, *Energy Environ. Sci.*, 2018, **11**, 3010–3018.
18 H. D. Pratt, N. S. Hudak, X. Fang and T. M. Anderson, *J. Power Sources*, 2013, **236**, 259–264.
19 K. Piepgrass and M. T. Pope, *J. Am. Chem. Soc.*, 1987, **109**, 1586–1587.
20 G. Hervé, *Ann. Chim.*, 1971, 287–296.
21 G. Hervé, *Ann. Chim.*, 1971, **6**, 219–228.
22 J. Canny, F.-X. Liu and G. Hervé, *C. R. Chimie*, 2005, **8**, 1011–1016.
23 M. H. Dickman, T. Ozeki, J. Howard T. Evans, C. Rong, G. B. Jameson and M. T. Pope, *J. Chem. Soc., Dalton Trans.*, 2000, 149–154.
24 J. P. Launay, *J. Inorg. Nucl. Chem.*, 1976, **38**, 807–816.
25 P. Souchay and J. Launay, *C. R. Acad. Sc.*, 1969, **268**, 1354–1357.
26 R. Contant, J.-M. Fruchart, G. Hervé and R. Massart, *C. R. Acad. Sc.*, 1970, **270**, 1952–1955.
27 T. Yamase and E. Ishikawa, *J. Chem. Soc., Dalton Trans.*, 1996, 1619–1627.
28 C. Boskovic, M. Sadek, R. T. C. Brownlee, A. M. Bond and A. G. Wedd, *J. Chem. Soc., Dalton Trans.*, 2001, 187–196.
29 N. I. Gumerova and A. Rompel, *Nat. Rev. Chem.*, 2018, **2**, 1–20.
30 X. López, C. Bo and J. M. Poblet, *J. Am. Chem. Soc.*, 2002, **124**, 12574–12582.
31 Y. Iwase, O. Tomita, H. Naito, M. Higashi and R. Abe, *J. Photochem. Photobiol. A: Chem.*, 2018, **356**, 347–354.
32 S. P. E. Smith, J. B. Christian, *Electrochim. Acta*, 2008, **53**, 2994–3001.
33 A. Kaur, G. Hundal and M. S. Hundal, *Cryst. Growth Des.*, 2013, **13**, 3996–4001.
34 A. Kobayashi and Y. Sasaki, *Bull. Chem. Soc. Jap.*, 1975, **48**, 885–888.
35 J. Malito, in *Annual Reports on NMR Spectroscopy*, ed. G. A. Webb, Academic Press, 1996, vol. 33, pp. 151–206.
36 S. F. Gheller, T. W. Hambley, R. T. C. Brownlee, M. J. O'Connor, M. R. Snow and A. G. Wedd, *J. Am. Chem. Soc.*, 1983, **105**, 1527–1532.
37 A. Nagasawa, Y. Sasaki, B. Wang, S. Ikari and T. Ito, *Chem. Lett.*, 1987, **16**, 1271–1274.
38 C. Sanchez, J. Livage, J. P. Launay, M. Fournier and Y. Jeannin, *J. Am. Chem. Soc.*, 1982, **104**, 3194–3202.
39 C. Falaise, M. A. Moussawi, S. Floquet, P. A. Abramov, M. N. Sokolov, M. Haouas and E. Cadot, *J. Am. Chem. Soc.*, 2018, **140**, 11198–11201.
40 C. Falaise, S. Khlifi, P. Bauduin, P. Schmid, W. Shepard, A. A. Ivanov, M. N. Sokolov, M. A. Shestopalov, P. A. Abramov, S. Cordier, J. Marrot, M. Haouas and E. Cadot, *Angew. Chem. Int. Ed.*, 2021, **60**, 14146–14153.
41 S. Khlifi, J. Marrot, M. Haouas, W. E. Shepard, C. Falaise and E. Cadot, *J. Am. Chem. Soc.*, 2022, **144**, 4469–4477.
42 A. Solé-Daura, V. Goovaerts, K. Stroobants, G. Absillis, P. Jiménez-Lozano, J. M. Poblet, J. D. Hirst, T. N. Parac-Vogt and J. J. Carbó, *Chem. Eur. J.*, 2016, **22**, 15280–15289.
43 T. Buchecker, P. Schmid, S. Renaudineau, O. Diat, A. Proust, A. Pfitzner and P. Bauduin, *Chem. Commun.*, 2018, **54**, 1833–1836.
44 K. I. Assaf and W. M. Nau, *Angew. Chem. Int. Ed.*, 2018, **57**, 13968–13981.
45 S. Yao, C. Falaise, A. A. Ivanov, N. Leclerc, M. Hohenschutz, M. Haouas, D. Landy, M. A. Shestopalov, P. Bauduin and E. Cadot, *Inorg. Chem. Front.*, 2021, **8**, 12–25.
46 S. Yao, C. Falaise, S. Khlifi, N. Leclerc, M. Haouas, D. Landy and E. Cadot, *Inorg. Chem.*, 2021, **60**, 7433–7441.
47 E. Schreiber, A. A. Fertig, W. W. Brennessel and E. M. Matson, *J. Am. Chem. Soc.*, 2022, **144**, 5029–5041.
48 E. Schreiber, B. E. Petel and E. M. Matson, *J. Am. Chem. Soc.*, 2020, **142**, 9915–9919.
49 K. Piepgrass and M. T. Pope, *J. Am. Chem. Soc.*, 1989, **111**, 753–754.